Available online at www.sciencedirect.com
ScienceDirect
Solar Energy 85 (2011) 1091–1100
SOLAR ENERGY
www.elsevier.com/locate/solener

Accurate altitude–azimuth tracking angle formulas for a heliostat with mirror–pivot offset and other fixed geometrical errors

Minghuan Guo, Zhifeng Wang *, Jianhan Zhang, Feihu Sun, Xiliang Zhang

Key Laboratory of Solar Thermal Energy and Photovoltaic System of Chinese Academy of Sciences, Institute of Electrical Engineering, Beijing 100190, China

Received 26 October 2010; received in revised form 28 February 2011; accepted 2 March 2011
Available online 31 March 2011

Communicated by: Associate Editor L. Vant-Hull

Abstract

High precision tracking formulas were developed for a receiver-oriented toroidal heliostat with the standard spinning-elevation tracking geometry in a previous paper. The spinning-elevation tracking geometry included some mirror–pivot offset, orthogonal intersecting rotational axes and the elevation axis being parallel to the mirror surface plane. This paper analyzes the tracking accuracy of these standard spinning elevation tracking formulas to show that they are accurate with negligible tracking error. Hence, the mirror-surface-center normal obtained from these formulas is accurate for any dual-axis tracking heliostat. Then, the accurate mirror-surface-center normal information is used to determine general altitude–azimuth tracking angles for a heliostat with a mirror–pivot offset and other geometrical errors. The main geometrical errors in a typical altitude–azimuth tracking geometry are the azimuth axis tilt from the vertical, the non-orthogonality between the two heliostat rotational axes, the non-parallel degree between the mirror surface plane and the altitude axis, and the encoder reference errors. An actual heliostat in a solar field is used as an example to demonstrate use of the general altitude–azimuth tracking formulas, with the tracking angles for this heliostat on typical days graphically illustrated. The altitude–azimuth tracking angle formulas are further verified by an indoor laser-beam tracking test on a specially designed heliostat model.

Keywords: Heliostat; Tracking; Mirror–pivot offset; Geometrical errors

1. Introduction

The solar field of a central receiver system (CRS) is composed of an array of heliostats on the ground beside or around a central tower, with each heliostat tracking the sun on two axes to continuously reflect the solar beam onto the fixed tower-top receiver. The concentrated solar radiation is absorbed by the receiver and then removed by the working fluid through tubes. The dual-axis sun tracking of each heliostat is very important for their optical performance. The primary axis of the dual-axis tracking is fixed to the foundation, with the secondary axis, which is fixed with respect to the mirror surface and parallel to the mirror surface plane, is perpendicular to the primary axis and rotates around it. As mentioned in the literature (Lipps and Vant-Hull, 1978), there are a number of heliostat dual-axis sun tracking modes, such as altitude–azimuth, radial–pitch–roll, azimuth–pitch–roll, polar and receiver-oriented. The altitude–azimuth tracking mode is most commonly used in solar engineering systems with the azimuth axis as the primary axis, which is naturally vertical, and the altitude axis as the secondary axis. The pitch–roll tracking mode (primary axis is horizontal) has the potential to permit a more compact array of heliostats than the altitude–azimuth tracking (Schramek and Mills, 2004). Zaibel et al. (1995) considered a combination of receiver oriented dual-axis tracking and a toroidal surface which used a toroidal surface with different sagittal and tangential radii at the vertex to reduce the astigmatism of the spherical mirror for the non-normal solar incidence. Receiver

* Corresponding author. Tel.: +86 10 62520684; fax: +86 10 62587946.
E-mail address: zhifeng@vip.sina.com (Z. Wang).

0038-092X/$ - see front matter
doi:10.1016/j.solener.2011.03.003

Nomenclature

O	heliostat pivot (heliostat rotation center)
T	aim point or receiver aperture center
M	mirror surface center (orthogonal projection of the heliostat pivot on the mirror surface plane)
OT, $\vec{t}$	spinning axis vector of a receiver-oriented tracking heliostat or the vector from **O** to **T**; $\vec{t}$ is the unit vector of **OT**
λ, φ	altitude and azimuth angles of **OT** (°)
ON, $\vec{n}$	mirror-surface-center normal and its unit vector
OS, $\vec{s}$	solar vector and its unit vector
α_s, A_s	solar altitude angle and solar azimuth angle along the north-to-east direction (°)
Φ	local latitude, northward is positive (°)
L_{loc}	local longitude, eastward is positive (°)
L	length of **OT** (m)
H_z	mirror–pivot offset from the heliostat pivot to the mirror surface plane (m)
L/H_z	ratio of L to H_z
θ'	elevation tracking angle for the standard spinning-elevation tracking (°)
ρ	right-hand spinning angle for the standard spinning-elevation tracking (°)
θ	nominal incident angle equal to the mirror-surface-center incident angle and elevation angle of the standard spinning-elevation tracking when there is no mirror–pivot offset (°)
θ^*	mirror-surface-center incident angle of the solar beam, $\theta' + \theta^* = 2\theta$ (°)
τ	elevation angle correction for the standard spinning-elevation tracking with a mirror–pivot offset, $\theta' = \theta - \tau$ and $\theta^* = \theta + \tau$ (°)
ε	tracking error of the standard spinning-elevation tracking, and also the tracking error of the altitude–azimuth tracking angle formulas (°)
γ, α	azimuth tracking angle and the altitude tracking angle for the altitude–azimuth tracking mode (°)
ψ_t, ψ_a	tilt angle and tilt azimuth angle of the azimuth axis from the vertical direction for altitude–azimuth tracking (°)
τ_1	dual-axis non-orthogonal angle, i.e. the bias angle of the altitude axis from the orthogonal position of the azimuth axis in the dual-axis plane $\mathbf{II}_1$ (°)
μ	canting angle of the mirror surface plane relative to the altitude axis, i.e. the angle between the mirror surface plane and the altitude axis (°)
$\|\cdot\|$	Norm or length of a vector, i.e. $\|(v_1, v_2, v_3)\| = \sqrt{v_1^2 + v_2^2 + v_3^2}$

oriented tracking is also called spinning-elevation tracking (Chen et al., 2001), since its spinning axis is the primary axis which points to the receiver and the elevation axis is the secondary axis. A special case of the receiver oriented dual-axis tracking is polar tracking where the primary axis is parallel to the polar axis of the earth and rotates at a constant clockwise speed, but this tracking mode is only used for an isolated mirror rather than a CRS.

When the two orthogonal rotational axes of a heliostat intersect (called the heliostat pivot) at the mirror surface center and the heliostat pivots around this point, then the mirror normal, $\vec{n}$, at the mirror surface center during sun tracking can be computed as $\vec{n} = (\vec{s} + \vec{t})/\|\vec{s} + \vec{t}\|$. Here, the vector $\vec{s}$ points to the sun while $\vec{t}$ points to the fixed aim point at the mirror surface center. The tracking angles of the primary and the secondary axes can then be easily derived from the vector components of $\vec{n}$ and the heliostat tracking geometry.

In practice, there is normally some offset between the mirror surface plane and the secondary rotational axis of the heliostat. However, there are no known exact altitude–azimuth tracking angle formulas available for a heliostat that account for the mirror–pivot offset. The difficulty in deriving the exact tracking formulas for the heliostat with mirror–pivot offset is that the mirror surface center is always moving during sun tracking.

In addition, a real altitude–azimuth tracking heliostat also suffers from geometrical errors due to mechanism imperfections. Thus, typical geometrical errors should also be taken into account when deriving the exact altitude–azimuth tracking formulas. Stone and Jones (1999) described a number of tracking error sources, including the three dominant geometric error sources as the azimuth axis tilt error (also called the pedestal tilt error), the mirror alignment error (or mirror canting error) and the encoder reference errors, and their effects on heliostat tracking. Although Chong and Wong (2009) presented a general formula for an on-axis sun-tracking system with three additional angular parameters, it only compensates for the dual-axis tracking effect of the azimuth axis tilt error for a sun tracker and is limited to the most commonly used simple solar vector (see Eqs. (24) and (25) in this paper).

This paper presents the accurate general altitude–azimuth tracking formulas for a heliostat with both a mirror–pivot offset and other fixed geometric errors. Here, the mirror alignment error does not refer to canting of the mirror facets, but to the bias of the mirror-surface-center normal from the expected direction. Since the angular component of the mirror-surface-center normal is indistinguishable from an altitude-axis encoder reference error, the mirror alignment error here is interpreted as the non-parallel degree of the entire mirror surface plane relative to the altitude axis, i.e.

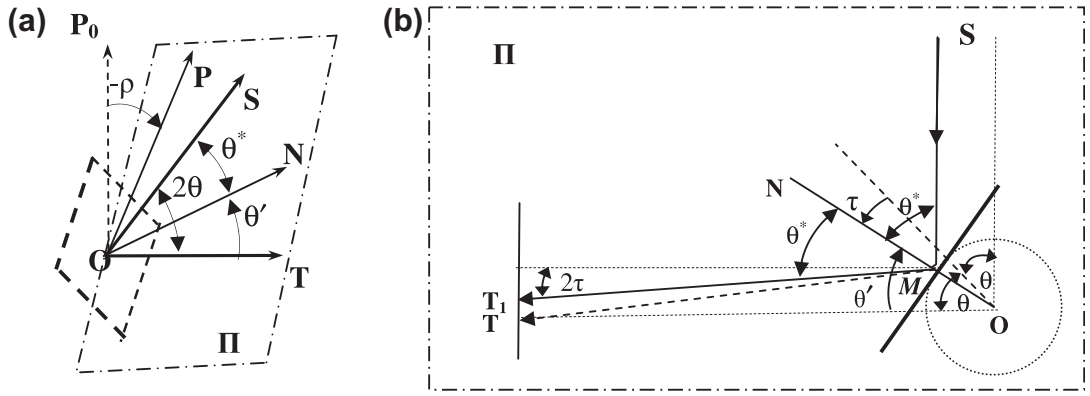

Fig. 1. Schematic of the standard spinning-elevation tracking geometry for a heliostat with a mirror–pivot offset. (a) spinning-elevation tracking geometry (without the mirror–pivot offset); (b) angular relationships and tracking error in the sun beam incidence plane.

the canting angle between the mirror surface plane and the altitude axis. The two rotational axes of a heliostat also may not be exactly orthogonal, so the bias angle between the altitude axis (secondary axis) and the orthogonal to the azimuth axis is also included in the altitude–azimuth tracking angle formulas. Since the encoder reference errors for the azimuth axis and the altitude axis have no direct relationship with the altitude–azimuth tracking geometry, the encoder reference errors are not considered in deriving the accurate altitude–azimuth tracking angle formulas for a heliostat with a mirror–pivot offset.

These altitude axis encoder reference and azimuth axis encoder reference have to be determined when applying the accurate altitude–azimuth tracking angle formulas to a real heliostat. A laser beam altitude–azimuth tracking test will be used to demonstrate use of the altitude–azimuth tracking angle formulas for a specially designed heliostat model and how to determine the encoder references.

2. Accurate mirror-surface-center normal of a heliostat with mirror–pivot offset

Guo et al. (2010) presented high precision spinning-elevation tracking formulas to calibrate the effect of the mirror–pivot offset for the standard spinning-elevation tracking geometry, which assumed that rotational axes were orthogonal and the elevation axis (secondary axis) was parallel to the mirror surface plane (tangential plane of the mirror surface at the mirror surface center). As the heliostat tracks the sun, the line connecting the heliostat pivot and the mirror surface center always coincides with the mirror-surface-center normal. Both spinning-elevation tracking and altitude–azimuth tracking should have the same mirror normal at the mirror surface center. Guo et al. (2010) did not give an expression of the expected mirror normal at the mirror surface center, so the spinning-elevation tracking formulas are developed further here to clearly identify the mirror-surface-center normal for a normal sun-tracking heliostat with a mirror–pivot offset.

2.1. Standard spinning-elevation tracking formulas for a heliostat with a mirror–pivot offset

The spinning-elevation tracking geometry is shown in Fig. 1 where point **O** stands for the heliostat pivot, with vectors **OT**, **ON**, **OS** being the spinning axis pointing to the aim point **T**, the mirror-surface-center normal and the solar vector. The upward vector $\mathbf{OP}_0$ perpendicular to **OT** is at the zero spinning position and the zero-position sun tracking plane of the heliostat containing $\mathbf{OP}_0$ and **OT** is perpendicular to ground plane. The sun beam incident plane **Π** is also the current tracking plane of the spinning axis and the vectors **OS**, **OP**, **OT** and **ON** are all within **Π**. ρ is the right-hand spinning angle around **OT** when $\mathbf{OP}_0$ moves to **OP**, i.e. $\angle\mathbf{P_0OP} = -\rho$. θ is the nominal sun beam incident angle, the elevation angle $\angle\mathbf{TON} = \theta'$, and $\theta^* = 2\theta - \theta'$ is the incident angle at the mirror surface center **M**. The elevation axis perpendicular to **Π** and the mirror–pivot offset are not drawn in Fig. 1a.

As Fig. 1b shows, the mirror surface center **M** is the orthogonal projection of the heliostat pivot **O** on the mirror surface plane in the sun beam incident plane Π, the mirror–pivot offset $\|\mathbf{OM}\| = H_z$, the slant distance $\|\mathbf{OT}\| = L$, **O**, **M** and **N** are collinear, τ is the elevation angle correction, $\theta' = \theta - \tau$ is the elevation tracking angle at **M** and $\theta^* = \theta + \tau$ is the sun beam incident angle at **M**. $\mathbf{T}_1$ is the intersection of the reflected sun beam from **M** with the image plane perpendicular to the spinning axis **OT** for a given nominal sun beam incident angle θ.

If the unit vectors for the vectors $\mathbf{OP}_0$, **OS**, **OP**, **OT** and **ON** are denoted as $\vec{p}_o, \vec{s}, \vec{t}$ and $\vec{n}$, then the following equations hold in the left-hand coordinate system [**O**; North-East-Height]:

$$\vec{s} = (\cos\alpha_s \cos A_s, \cos\alpha_s \sin A_s, \sin\alpha_s) \tag{1}$$

$$\vec{t} = (\cos\lambda\cos\varphi, \cos\lambda\sin\varphi, \sin\lambda) \tag{2}$$

$$\vec{p}_0 = (-\sin\lambda\cos\varphi, -\sin\lambda\sin\varphi, \cos\lambda) \tag{3}$$

$$\theta = 0.5\arccos(\vec{s}\cdot\vec{t}) = 0.5\arccos(\sin\lambda\sin\alpha_s + \cos\lambda\sin\varphi\cos\alpha_s\sin A_s + \cos\lambda\cos\varphi\cos\alpha_s\cos A_s) \quad (4)$$

$$\begin{cases} \rho = \arccos\{[-\sin\lambda\cos\alpha_s\cos(A_s-\varphi) + \cos\lambda\sin\alpha_s]/\sin(2\theta)\}, & \text{if } \sin(A_s-\varphi)\geq 0 \\ \rho = -\arccos\{[-\sin\lambda\cos\alpha_s\cos(A_s-\varphi) + \cos\lambda\sin\alpha_s]/\sin(2\theta)\}, & \text{if } \sin(A_s-\varphi)\leq 0 \end{cases} \quad (5)$$

$$\vec{p} = (\vec{s} - \cos(2\theta)\,\vec{t})/\sin(2\theta) \quad (6)$$

$$\vec{n} = \cos\theta' + \sin\theta'\,\vec{p} = (\sin\theta'\,\vec{s} + \sin\theta^*\,\vec{t})/\sin(2\theta), \quad (\vec{n}=\vec{s} = \vec{t},\ \text{when } \theta = 0^\circ). \quad (7)$$

Here, α_s is the solar altitude angle and A_s is the solar azimuth angle. Likewise, λ is the altitude angle of **OT** and φ is the azimuth angle of **OT** in the north-to-east direction.

Guo et al. (2010) derived the elevation angle inside plane **Π** for a receiver-oriented heliostat with mirror–pivot offset H_z in terms of the nominal sun beam incident angle θ as

$$\begin{cases} \theta' = \theta - \tau \\ \tau = \arcsin\left(\frac{H_z\sin\theta}{2L - H_z\cos\theta}\right) \end{cases} \quad (8)$$

Thus, the standard spinning-elevation tracking formulas are mainly Eqs. (4), (5), and (8) with Eq. (7) for the mirror-center normal vector.

2.2. Exactness of the mirror-surface-center normal

The angle between **MT** and $\mathbf{MT}_1$, ε, is the tracking error in terms of θ and τ, as can be seen in Fig. 1b. From Eq. (8), τ is determined by θ and L/H_z, so the tracking error ε is a two-variable function of θ and L/H_z. L/H_z is the ratio of the heliostat slant distance to the mirror–pivot offset. ε is computed from:

$$\cos\epsilon = (\mathbf{MT}\cdot\vec{t}_1)/\|\mathbf{MT}\| \quad (9)$$

$$\vec{t} = \mathbf{MT}_1/\|\mathbf{MT}_1\| = -\vec{s} + (2\cos\theta^*)\,\vec{n} \quad (10)$$

$$\vec{n} = (\sin\theta'\,\vec{s} + (\sin\theta^*\,\vec{t})/\sin(2\theta) \quad (11)$$

$$\mathbf{MT} = \mathbf{OT} - \mathbf{OM} = L\,\vec{t} - H_z\,\vec{n}. \quad (12)$$

The elevation angle correction, τ, calculated from Eq. (8) is shown in Fig. 2a. The maximum τ is 1.8157°. The tracking error ε computed using Eq. (9)–(12) is shown in Fig. 2b. The maximum ε is 2.50e−5°, which is much less than the maximum solar vector error (smaller than 0.0003°) of SPA (solar position algorithm) (Reda and Andreas, 2004). Moreover, the minimum L/H_z in a typical CRS solar field is generally greater than 100. Therefore, the high precision spinning-elevation tracking formulas in Eqs. (4), (5), and (8) are sufficiently accurate for a heliostat with a reasonable mirror–pivot offset, $\mathbf{T}_1$ and **T** are essentially the same point, and Eq. (11) accurately represents the mirror-surface-center normal for the heliostat.

Since the position of the mirror surface center, **M**, is determined by the mirror-surface-center normal $\vec{n}$, $\mathbf{OM} = H_z\,\vec{n}$ in Eq. (12), accurate tracking angle formulas for a heliostat with a mirror–pivot offset can be derived by simply transposing the mirror-surface-center normal to the corresponding dual-axis tracking angles for the specific heliostat tracking geometry, such as the altitude–azimuth dual-axis tracking geometry used in this paper.

3. Altitude–azimuth tracking formulas for a heliostat with mirror–pivot offset

Altitude–azimuth tracking formulas are developed which include the azimuth axis tilt from the vertical, the non-orthogonality of the two rotational axes and the non-parallel degree of the mirror surface plane to the altitude axis.

Fig. 3 shows the altitude–azimuth tracking geometry for a heliostat with a mirror–pivot offset, where the mirror-surface-center normal **ON** is always collinear with the line connecting the heliostat pivot **O** and the mirror surface center **M**. In Fig. 3, ψ_t is the tilt angle and ψ_a is the tilt azimuth angle of the heliostat pedestal; $\mathbf{\Pi}_1$ is the dual-axis plane containing the azimuth axis and the altitude axis, τ_1 is the bias angle of the altitude axis from the orthogonal to the azimuth axis, $\mathbf{\Pi}_2$ is the plane determined by the altitude axis and the mirror surface center **M**, and μ is the canting angle of the mirror surface plane relative to the altitude axis. The azimuth axis rotates in the left-hand direction, while the altitude axis rotates in the right-hand direction. Here, the tracking angle for the azimuth axis is γ while that for the altitude axis is α. $\mathbf{\Pi}_2$ is also the E_1–E_2 plane of the local left-hand Cartesian coordinate system [**O**; E_1–E_2–E_3].

The E_1–E_2–E_3 coordinates of the mirror-surface-center normal **ON** are (cos μ, sin μ, 0). The mirror-surface-center normal $\vec{n} = (n_1, n_2, n_3)$ in [**O**; North-East-Height] obtained from Eqs. (4), (8), and (7) can be transformed into (cos μ, sin μ, 0) through six rotational transformation matrices applied in order. Equivalently, the North axis can be moved to the E_1 axis by six successive rotational transformations using the left-hand rule from coordinate system [**O**; North-East-Height] to the local coordinate system [**O**; E_1–E_2–E_3]. These rotational transformation matrices are:

$$B_1 = B_1(3,\psi_a) = \begin{bmatrix} \cos\psi_a & \sin\psi_a & 0 \\ -\sin\psi_a & \cos\psi_a & 0 \\ 0 & 0 & 1 \end{bmatrix},$$

$$B_2 = B_2(2,\psi_t) = \begin{bmatrix} \cos\psi_t & 0 & -\sin\psi_t \\ 0 & 1 & 0 \\ \sin\psi_t & 0 & \cos\psi_t \end{bmatrix},$$

$$B_3 = B_3(3,-\psi_a) = \begin{bmatrix} \cos\psi_a & -\sin\psi_a & 0 \\ \sin\psi_a & \cos\psi_a & 0 \\ 0 & 0 & 1 \end{bmatrix},$$

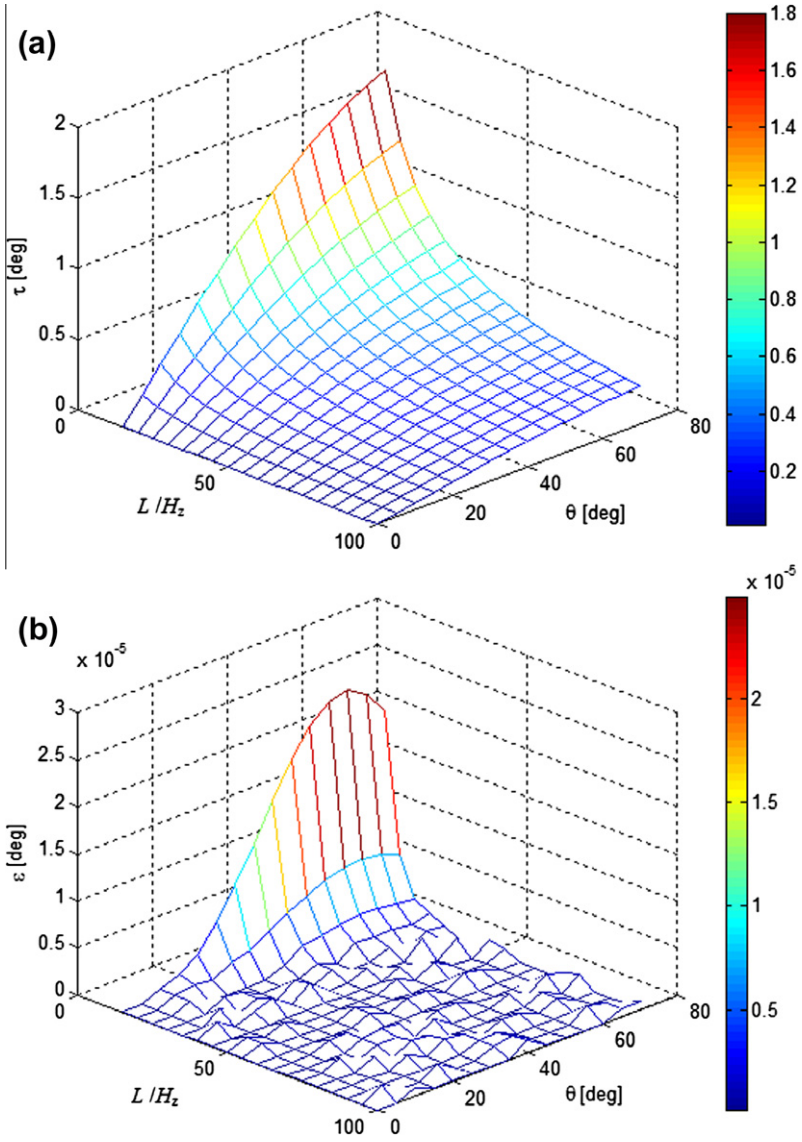

Fig. 2. Grid-data tracking error of standard spinning-elevation tracking. (a) elevation angle correction τ, (b) tracking error ε.

$$B_4 = B_4(3,\gamma) = \begin{bmatrix} \cos\gamma & \sin\gamma & 0 \\ -\sin\gamma & \cos\gamma & 0 \\ 0 & 0 & 1 \end{bmatrix},$$

$$B_5 = B_5(1,\tau_1) = \begin{bmatrix} 1 & 0 & 0 \\ 0 & \cos\tau_1 & \sin\tau_1 \\ 0 & -\sin\tau_1 & \cos\tau_1 \end{bmatrix},$$

$$B_6 = B_6(2,-\alpha) = \begin{bmatrix} \cos\alpha & 0 & \sin\alpha \\ 0 & 1 & 0 \\ -\sin\alpha & 0 & \cos\alpha \end{bmatrix},$$

$B_1(3, \psi_a)$ is the initial coordinate system ([**O**; North-East-Height]) to a new coordinate system position around the 3rd axis through the angle ψ_a in the left-hand direction. $B_2(2, \psi_t)$ then further rotates the result of the $B_1(3, \psi_a)$ rotation to the next coordinate system position around the 2nd axis through the angle ψ_t in the positive left-hand direction. $B_3(3, -\psi_a)$, $B_4(3, \gamma)$, $B_5(1, \tau_1)$ and $B_6(2, -\alpha)$ are similar rotations where '$-\psi_a$' in B_3 and '$-\alpha$' in B_6 stand for the rotation angles ψ_a and α in the right-hand direction.Thus, the altitude–azimuth tracking equation is

$$(\cos\mu, \sin\mu, 0)^T = B_6B_5B_4B_3B_2B_1(n_1, n_2, n_3)^T. \quad (13)$$

Eq. (13) can be rewritten as

$$(B_5)^T(B_6)^T(\cos\mu, \sin\mu, 0)^T = B_4[B_3B_2B_1(n_1, n_2, n_3)^T] \quad (14)$$

Defining

$$(c_1, c_2, c_3)^T = B_3B_2B_1(n_1, n_2, n_3)^T \quad (15)$$

then

$$\begin{aligned} B_4[B_3B_2B_1(n_1, n_2, n_3)^T] &= B_4(c_1, c_2, c_3)^T \\ &= (c_1\cos\gamma + c_2\sin\gamma, c_2\cos\gamma \\ &\quad - c_1\sin\gamma, c_3)^T \end{aligned} \quad (16)$$

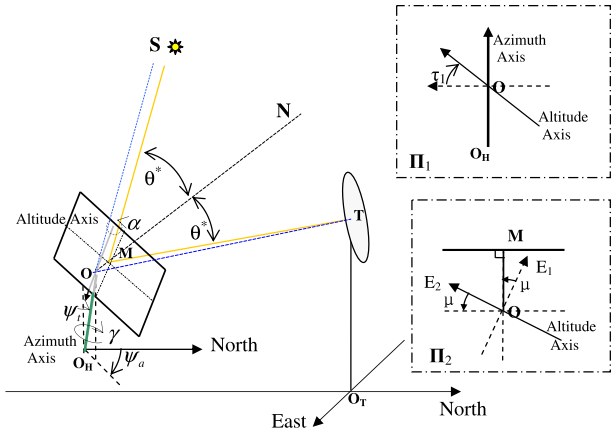

Fig. 3. Altitude–azimuth tracking geometry for a heliostat with a mirror–pivot offset. The left-hand azimuth axis and the right-hand altitude axis are the primary and secondary axes. γ and α are the azimuth and altitude tracking angles of the altitude–azimuth tracking heliostat. ψ_t and ψ_a are the tilt angles for the azimuth axis from the vertical direction. τ_1 is the bias angle of the altitude axis from the orthogonal to the azimuth axis. μ is the canting angle of the mirror surface plane relative to the altitude axis.

$$(B_5)^T(B_6)^T(\cos\mu,\sin\mu,0)^T = (\cos\mu\cos\alpha, \times\cos\tau_1\sin\mu-\sin\tau_1\cos\mu\sin\alpha, \times\sin\tau_1\sin\mu+\cos\tau 1\cos\mu\sin\alpha)^T \quad (17)$$

Comparing Eqs. (16) and (17), the altitude–azimuth tracking angles α and γ are:

$$\alpha = \arcsin\{(c_3-\sin\tau_1\sin\mu)/(\cos\tau_1\cos\mu)\} \quad (18)$$

$$d_1 = \cos\mu\cos\alpha \quad (19)$$

$$d_2 = \cos\tau_1\sin\mu-\sin\tau_1\cos\mu\sin\alpha \quad (20)$$

$$\cos\gamma = (c_1d_1+c_2d_2)/(c_1^2+c_2^2), \quad (21)$$

$$\sin\gamma = (c_2d_1-c_1d_2)/(c_1^2+c_2^2), \quad (22)$$

$$\begin{cases} \gamma = \arccos\{(c_1d_1+c_2d_2)/(c_1^2+c_2^2)\}, \\ \quad \text{if } (c_2d_1-c_1d_2)\geq 0 \\ \gamma = 360^\circ-\arccos\{(c_1d_1+c_2d_2)/(c_1^2+c_2^2)\}, \\ \quad \text{if } (c_2d_1-c_1d_2)<0 \end{cases} \quad (23)$$

when $\psi_t = 0°$, $\tau_1 = 0°$, $\mu = 0°$, $\gamma = 0°$ and $\alpha = 0°$, the heliostat is in the vertical position with the mirror-surface-center normal $\vec{n}$ horizontal and pointing exact to North, i.e. $\vec{n} = (1,0,0)$. The set of expressions in Eqs. (4), (8), (7), (15), (18), (19), (20), (21), (22), and (23) are the altitude–azimuth tracking angle formulas for a heliostat with a mirror–pivot offset.

4. Application of the altitude–azimuth tracking formulas to a specific heliostat in solar field

To check the validity of the altitude–azimuth tracking angle formulas, the formulas are applied to a typical heliostat in a solar field in Beijing to simulate the dual-axis tracking angles on typical days. These altitude–azimuth tracking angle curves show the effect of the altitude–azimuth tracking formulas for a heliostat with mirror–pivot offset, azimuth axis tilt error, non-orthogonality of rotational axes, and non-parallel mirror surface plane relative to the altitude axis.

4.1. Solar angles for typical days

The longitude of the Beijing solar field is $L_{loc} = 115.9367°$E, the latitude is $\Phi = 40.3833°$N, the receiver aperture center, **T**, is 81.526 m high above the field ground plane, and the field has 110 heliostats. All the heliostat pivots are assumed to be 5.5 m above the ground plane and all the mirror–pivot offsets are assumed to be $H_z = 0.86$ m.

The solar vector algorithm is used for its simplicity,

$$\alpha_s = \arcsin(\sin\delta\sin\Phi+\cos\delta\cos\omega\cos\Phi) \quad (24)$$

$$A_s = 180^\circ + sign(\sin\omega)\arccos\left(\frac{\sin\alpha\sin\Phi-\sin\delta}{\cos\alpha\cos\Phi}\right) \quad (25)$$

where Φ is the site latitude (northward is positive), ω is the solar hour angle, and δ is the solar declination. ω and δ are computed using the expressions in the book by Duffie and Beckman (Duffie and Beckman, 1991).

The solar altitude angle, α_s, and the solar azimuth angle, A_s, calculated using Eqs. (24) and (25), for seven typical days of an average year are plotted in Fig. 4 to illustrate the changes of the solar angles in Beijing. "m12d21" means the 21st December with the other symbols referring to the other dates. The upper and the lower bounds of each time span for each day are to the nearest half hour. A_s is measured eastward from the north direction.

The No. 8 heliostat (#8) in the solar field was chosen to demonstrate the tracking angles from the altitude–azimuth tracking angle formulas for the solar angles in Fig. 4. Fig. 5 shows the position of the #8 heliostat in the solar field and the position of the receiver aperture center (tracking aim point). The #8 heliostat has $L = 131.67$ m, $H_z = 0.86$ m, $L/H_z = 153.1$, $\lambda = 35.269°$ and $\varphi = -163.76°$. The maximum and minimum L/H_z for all 110 heliostats in the solar field are 334.72 and 111.45. The maximum nominal incident angle, θ, is less than 66° for the solar angles shown in Fig. 4.

The maximum τ for the #8 heliostat for the solar angles shown in Fig. 4 based on Eq. (8) is less than 0.16°, while the maximum tracking error, ε, for the #8 heliostat based on Eq. (9) is less than $(1.708\times10^{-6})°$. This tracking error is essentially zero, which shows that the mirror-surface-center normal given by Eqs. (4), (8), and (11) is very accurate for the altitude–azimuth tracking of the #8 heliostat.

4.2. Simulated tracking angles from the altitude–azimuth tracking formulas

Consider the #8 heliostat, with azimuth axis tilt angles $\psi_t = 2°$ and $\psi_a = 78°$, dual-axis non-orthogonal angle

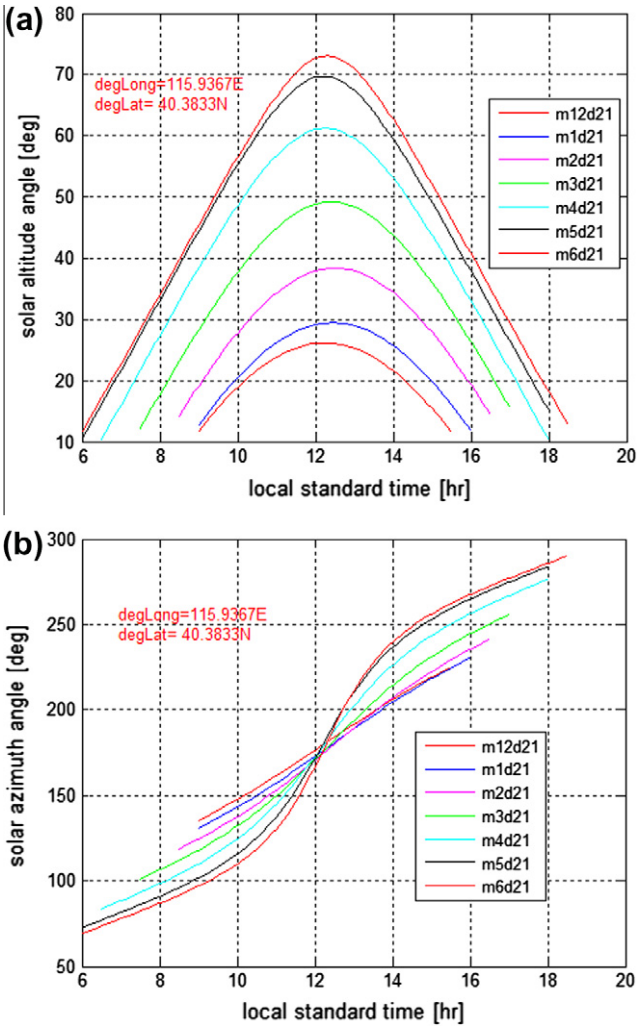

Fig. 4. Solar angle curves with respect to Beijing time on 21st December, 21st January, 21st February, 21st March, 21st April, 21st May and 21st June. (a) solar altitude angle, α_s, from Eq. (24); (b) solar azimuth angle, A_s, (in north-to-east direction) based on Eq. (25).

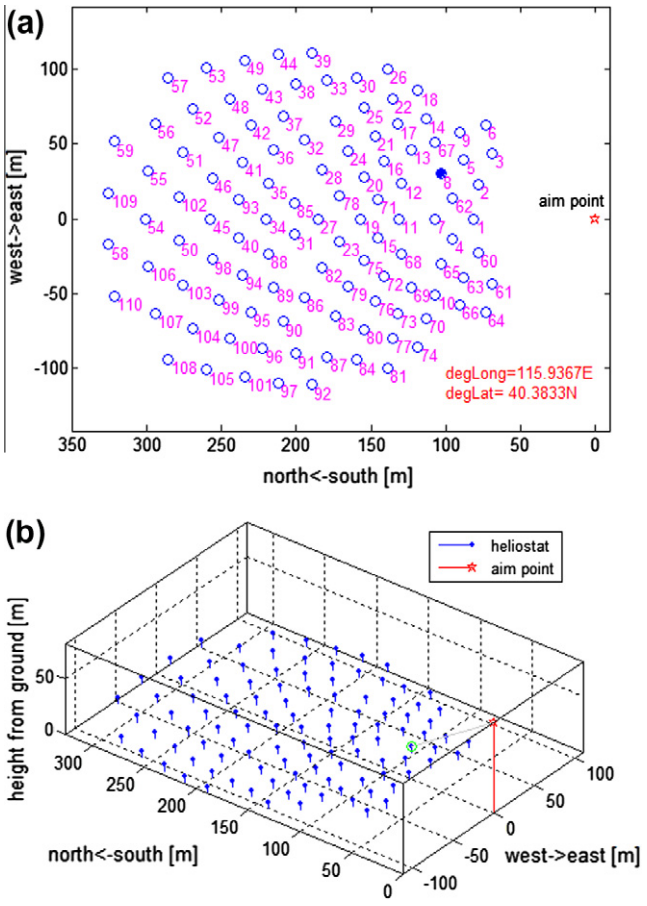

Fig. 5. Position of the #8 heliostat in the solar field. The aim point is the tower-top receiver aperture center. (a) plan view of the solar field and receiver, (b) 3D visualization of the geometric relationship between the #8 heliostat and the aim point.

$\tau_1 = -0.5°$, and canting angle $\mu = 1°$. The azimuth tracking angle, γ, and the altitude tracking angle, α, for the #8 heliostat and the solar angles shown in Fig. 4, based on Eqs. (23) and (18) are plotted in Fig. 6 which shows that the tracking angles on these days are not symmetric with respect to the time, but that the azimuth tracking angles are nearly equal at 11 A.M. Beijing time.

5. Laser beam test of the tracking formulas on a specially designed heliostat model

5.1. Test setup

A three-dimensional coordinate measuring machine (3D CMM) was used for laser beam tracking tests to verify the altitude–azimuth tracking formulas. A red semiconductor laser with good beam collimation was used at the CMM measuring head, so the vertically downward focused laser beam could be accurately moved along the X and Y directions either automatically or manually. The laser beam was used to simulate the sun beam, with the beam always parallel to the Z direction of the CMM. For the altitude–azimuth tracking formulas expressed in coordinate system [**O**; North-East-Height], the X, Y and Z directions of the CMM correlate to the East, North and Height directions.

Fig. 7 shows the tracking test apparatus used to evaluate the altitude–azimuth angle formulas with an automatically fixed-direction laser beam. The table heliostat model in Fig. 7a holds the azimuth motor with the azimuth axis perpendicular to the table plane and works as the heliostat pedestal. Two identical sloped bars with slope angles of 2° are laid parallel on the flat CMM platform. The four feet of the table rest on these two bars, so that the azimuth rotation axis of the heliostat model is tilted 2°from the zenith line. The altitude motor is fixed to the rotating shaft of the azimuth motor so that the altitude axis is not parallel to the table plane but tilts downward towards the table plane. A bar connected to the end of the altitude motor shaft connects to the flat glass mirror so that it is not exactly orthogonal to the altitude axis. The angle between the bar and the altitude axis is $(89 + 5/60)°$, i.e. the bar tilts

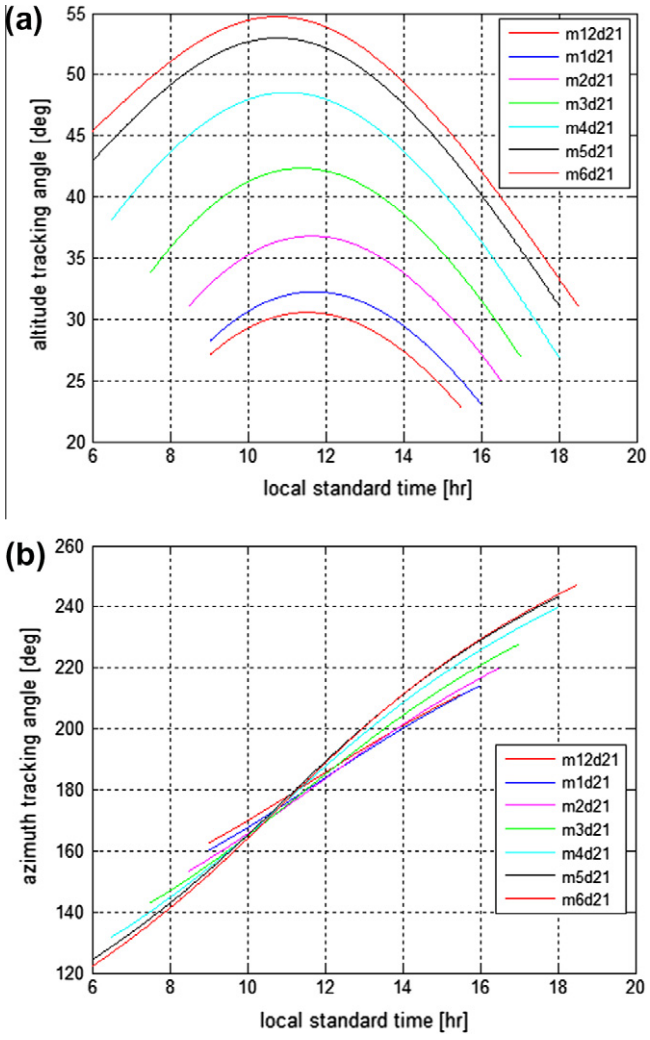

Fig. 6. Altitude tracking angle, α, and azimuth tracking angle, γ, for the #8 heliostat based on the altitude–azimuth tracking formulas Eqs. (18) and (23) corresponding to the solar angles in Fig. 4. (a) α and (b) γ.

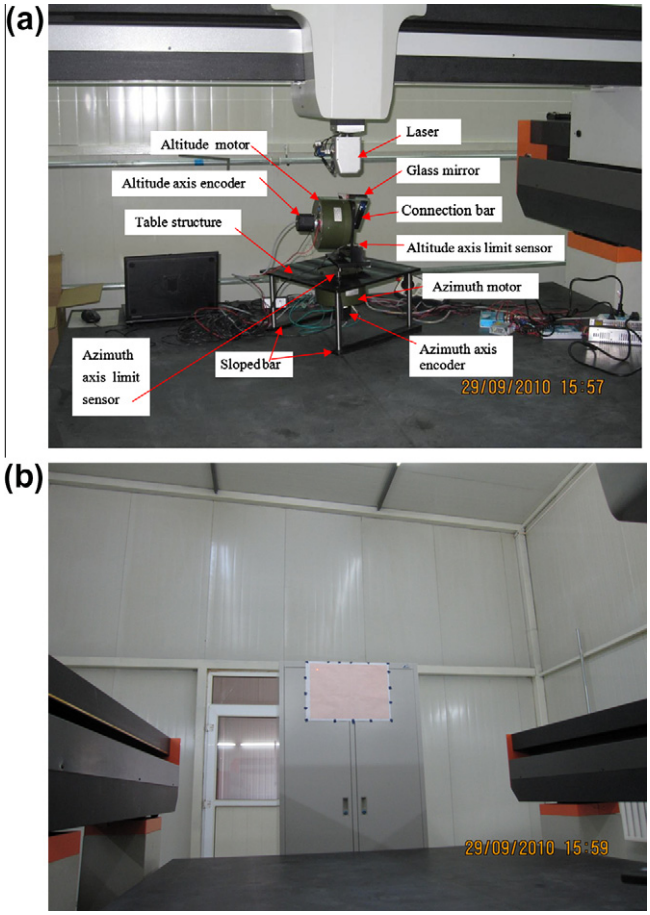

Fig. 7. Altitude–azimuth laser beam tracking test of the angle formulas on a heliostat model. (a) Geometry of the heliostat model and laser, (b) size and position of the target plane.

(1–5/60)° away from the front end plane of the altitude motor. The azimuth motor and the altitude motor are both 24 V DC torque motors with no reduction gears. The back end of each motor has an incremental photoelectric encoder, with a resolution of 5000 lines per revolution. For each tracking angle position for both drive motors, the motor always runs from its initial angle position (encoder reference) which is automatically identified by the rotation limit sensor of the regarding rotation axis. The flat glass mirror, which is glued to the top end of the bar, has a back glass layer 100 mm × 26 mm × 3 mm, with a back-silvered glass mirror 1 mm thick on top. The mirror surface center, which is the orthogonal projection on the mirror surface plane of the heliostat pivot, is marked by a black ink circle, to indicate if the laser beam is incident on the mirror surface center. A red laser is positioned over the heliostat model so that its X–Y position is the same as that of the mirror surface center in the course of normal laser beam dual-axis tracking of the heliostat model. This position can be easily calculated from the tracking geometry. The target rectangular box shown in Fig. 7b is placed on the floor at the South side of the CMM platform with a sheet of 500 mm × 350 mm coordinate paper as a tracking target plane attached to the front wall of the cabinet which exactly faces the horizontal North (Y direction). This paper gives a two-dimensional target coordinate system [$\mathbf{T}_0$; U–V], where the origin $\mathbf{T}_0$ is at the left-top corner of the grid area on the target paper, the horizontal U axis coincides with the West direction and the vertical V axis is in the negative Height direction.

In the coordinate system [**O**; North-East-Height], the origin **O** is the heliostat pivot, the laser beam vector $\vec{s} = (0, 0, 1)$, $\mathbf{T}_0 = 0.001\ \text{m} * (-2593.9,\ 348.76,\ 763.79)$, $H_z = 0.12915$ m, the azimuth axis tilt angles $\psi_t = 1.854°$ and $\psi_a = 236.06°$, the dual-axis non-orthogonal angle $\tau_1 = 5°$, and the canting angle $\mu = -(1\text{–}5/60)°$. The measured azimuth axis tilt angle $\psi_t = 1.854°$ does not equal the 2° slope angle of the two sloped bars, since the CMM platform is not exactly horizontal. The tilt angle and the tilt azimuth angle of the CMM platform are 0.22326° and 103.64° in the north-to-east direction, respectively.

Given an aim point $\mathbf{T}_i = (U_i, V_i)$ on the target plane, the corresponding aim point vector $\vec{t}_i$ in the coordinate system [**O**; North-East-Height] can be calculated as:

$$\vec{t}_i = (T_0(1), T_0(2) - U_i, T_0(3) - V_i)/\|(T_0(1), T_0(2) - U_i, T_0(3) - V_i)\|. \quad (26)$$

5.2. Laser beam altitude–azimuth tracking test

The zero angle positions of the azimuth axis encoder and the altitude axis encoder must be determined for the altitude–azimuth tracking formulas in Eqs. (4), (8), (7), (15), (18), (19), (20), (21), (22), and (23). In this case, the initial angle positions marked by the azimuth axis limit sensor and the altitude axis limit sensor are first used directly as the zero angle positions of the two encoders, and then the zero angle positions of the two tracking axes for $\alpha = 0°$ and $\gamma = 0°$ are to be accurately determined.

Since the physical resolution of the encoders is 5000 lines per revolution, i.e. $360°/5000 = 0.072°$, close to 0.1°, the interface software for the two servo drive controllers always truncates the input tracking angles to an accuracy of one decimal (i.e. 0.1°), although the fourfold frequency multiplication technique of these drive controllers can enhance the positioning accuracy of the two drive motors. To alleviate this effect of the limited encoder resolution, each tracking test first moved both motors to the desired angular positions with one-decimal accuracy, and then the laser beam was moved to the marked mirror surface center, with the position of the reflection of the laser beam on the target plane then noted.

The data for nine laser beam tracking tests is reported in Table 1. The U–V locations of the nine laser beam reflection points in the tracking tests listed in Table 1 are plotted in Fig. 8. These U–V coordinates of the nine reflected laser beam points on the target plane were then put into the Eqs. (4), (8), (7), (15), (18), (19), (20), (21), (22), and (23) to get the corresponding altitude tracking angles and azimuth tracking angles which are also listed in Table 1 for comparison. In Table 1, the U–V coordinates have units of mm, while in Eq. (26) the unit of U_i and V_i is meter. The altitude and azimuth tracking angles were taken directly from the altitude and azimuth axis encoders. The X–Y coordinates of the laser position which were equal to those coordinates of the mirror surface center were read from the CMM coordinate system.

For the nine set of tracking test data listed in Table 1, the mean and the standard deviation of the difference between the recorded and the computed altitude tracking angles are 22.832° and 0.011051°. Similarly, the mean and the standard deviation of the difference between the recorded and the computed azimuth tracking angles are −237.43°and 0.014302°, respectively.

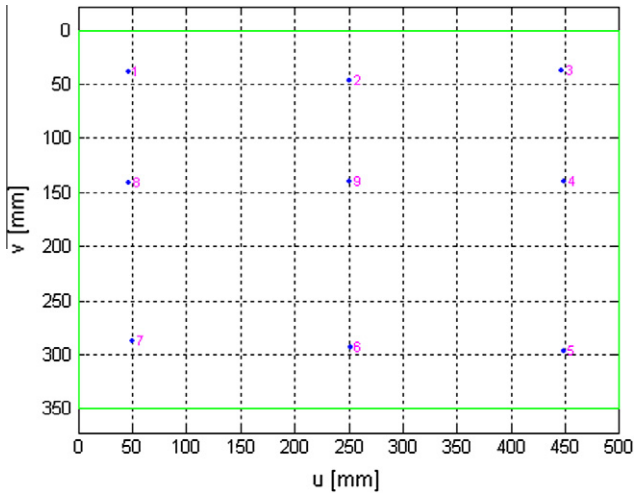

Fig. 8. Reflection points of the laser beam on the U–V target plane for the nine altitude–azimuth tracking tests.

Thus, $\alpha_0 = 22.832°$ was taken to be the zero angle position of the altitude axis, while $\gamma_0 = -237.43°$ was taken to be the zero angle position of the azimuth axis. In this case, the initial tracking angles for the altitude axis limit sensor and the azimuth axis limit sensor are $-\alpha_0 = -22.832°$ and $-\gamma_0 = 237.43°$, respectively.

Both the standard deviation of the altitude tracking angle difference (0.011051°) and the standard deviation of the azimuth tracking angle difference (0.014302°) are acceptable, which verifies the correctness of the altitude–azimuth tracking angle formulas. If these equations were not correct, the nine pairs of zero angle positions derived from these altitude–azimuth tracking angle formulas would not agree.

6. Conclusions

This paper presents accurate altitude–azimuth tracking angle formulas for a heliostat with a mirror–pivot offset. These formulas take into account the azimuth axis tilt from the vertical, the non-orthogonality of the two rotational axes and the non-parallel degree between the mirror surface plane

Table 1
Laser beam altitude–azimuth tracking test.

Test order	1	2	3	4	5	6	7	8	9
Recorded altitude angle (°)	76	76.1	76.3	75.2	73.5	73.4	73.3	74.9	75.1
Recorded azimuth angle (°)	−58.1	−53.5	−49	−49.2	−49.5	−54	−58.5	−58.3	−53.7
U of laser beam reflection (mm)	46	251	447	449	448.5	51.5	50	47	251
V of laser beam reflection (mm)	38	46	37	140	297	293	288	141	140
X coordinate of laser (mm)	−1007.9	−1014.1	−1019.7	−1020.3	−1020.4	−1013.9	−1007.5	−1007.7	−1014
Y coordinate of laser (mm)	−443.95	−444.48	−444.34	−446.25	−449.14	−449.12	−448.58	−445.85	−446.22
Computed altitude angle (°)	53.175	53.262	53.479	52.372	50.649	50.573	50.475	52.075	52.251
Computed azimuth angle (°)	179.32	183.94	188.41	188.24	187.9	183.44	178.92	179.14	183.74

and the altitude axis, so these altitude–azimuth tracking angle formulas are applicable to heliostats with both mirror–pivot offsets and other fixed geometric errors.

Simulated tracking angle curves for seven typical days given for the fixed position relationship between the #8 heliostat and the tower-top aim point are plotted to demonstrate these altitude–azimuth tracking formulas. These simulations provide insight into the tracking angle formulas and tracking using the altitude–azimuth tracking geometry.

Laser altitude–azimuth tracking tests using a specially designed heliostat model constructed on a 3D CMM platform have verified the altitude–azimuth tracking angle formulas.

More complicated dual-axis tracking geometries, such as when the primary rotational axis and the secondary rotational axis are not in a plane, and will have no intersection point; therefore, determination of the dual-axis tracking angle will require iterative methods. In this case, the line connecting the heliostat pivot and the mirror surface center no longer coincides with the mirror-surface-center normal.

Future work will study the effectiveness of these altitude–azimuth tracking formulas on real heliostats in the Beijing solar field.

Acknowledgements

This work was financed by China National Science and Technology Plan (973 Plan) project: large-scale solar thermal power system integration and control strategy (2010CB227104) and the China National Hi-Tech R&D (863 Plan) project: solar thermal power tower system, overall design and system integration technology (2006AA050101).

References

Chen, Y.T., Chong, K.K., Bligh, T.P., Chen, L.C., Yunus, J., Kannan, K.S., Lim, B.H., Lim, C.S., Alias, M.A., Bidin, N., Aliman, O., Salehan, S., Rezan, S.A.H. Shk. Abd., Tam, C.M., Tan, K.K., 2001. Non-imaging focusing heliostat. Sol. Energy 71 (3), 155–164.

Chong, K., Wong, C., 2009. General formula for on-axis sun-tracking system and its application in improving tracking accuracy of solar collector. Solar Energy 83 (3), 298–305.

Duffie, J.A., Beckman, W.A., 1991. Solar Engineering of Thermal Processes. John Wiley, New York, ISBN: 0471510564.

Guo, Minghuan, Wang, Zhifeng, Liang, Wenfeng, Zhang, Xiliang, Zang, Chuncheng, Lu, Zhenwu, We, Xiudong, 2010. Tracking formulas and strategies for a receiver oriented dual-axis tracking toroidal heliostat. Solar Energy 84, 939–947.

Lipps, F.W., Vant-Hull, L.L., 1978. A cellwise method for solar central receivers systems. Solar Energy 20, 505–516.

Reda, I., Andreas, A., 2004. Solar position algorithm for solar radiation applications. Solar Energy 76, 577–589.

Schramek, Philipp, Mills, David R., 2004. Heliostats for maximum ground coverage. Energy 29, 701–713.

Stone, K., Jones, S., 1999. Analysis of Solar Two Heliostat Tracking Error Sources. Tech. Rep. SAND99-0239c, Sandia, Albuquerque, New Mexico.

Zaibel, R., Dagan, E., Karni, J., Ries, H., 1995. An astigmatic corrected target-aligned heliostat for high concentration. Sol. Energy Mater. Sol. Cells 37, 191–202.